Wideband Single-Layer D-Band Patch Antenna with Parasitic Elements and Superstrate Loading

Yuyan Cao[1], Hanieh Aliakbari[1,2], Parisa Aghdam[3], Buon Kiong Lau[1]
[1] Department of Electrical and Information Technology, Lund University, Sweden, yu-yan.cao@eit.lth.se
[2] Volvo Car Corporation, Gothenburg, Sweden.
[3] Ericsson AB, Gothenburg, Sweden.

***Abstract*—This paper proposes a D-band patch antenna featuring four parasitic elements and a loaded superstrate layer. Inspired by a previous parasitic patch antenna design, the new structure is synthesized from scratch using characteristic mode analysis. The new design features different operating principles that enable low-cost single-layer fabrication on PCB HDI technology, while retaining wideband operation and high gain performance of the previous design. With the coupling between the active and parasitic patches limiting the bandwidth and radiation performance, a superstrate is added to improve the parasitic coupling and hence allowing a larger gap between the patches that fulfills fabrication requirements. The simulated results demonstrate that the antenna achieves 20.2% 10 dB impedance bandwidth and 9 dBi peak gain. The low cost and high performance make the design suitable for 6G applications.**

***Index Terms*—Patch antenna, D-band antenna, parasitic antenna, superstrate loading, characteristic mode analysis**

I. Introduction

6G is well positioned to enable new wireless applications that require extreme data rates, e.g., extended reality (XR) and holographic display. In particular, D-band (110-170 GHz), recognized for its ability to yield high-speed, low-latency and high-capacity communication, is becoming a hot topic [1], [2]. To fully leverage the potentials of D-band, optimizing antenna design is essential. However, unlike antenna design in sub-6 GHz bands, mm-wave bands (including D-band) present far more severe practical design challenges due to their much smaller wavelengths requiring far higher fabrication accuracy as well as higher frequencies needing more exotic materials to achieve high efficiency (see [2] and references therein).

To date, computer numerical control (CNC) machining, 3D printing, low temperature co-fired ceramics (LTCC), and high-density interconnect (HDI) processes have been explored to varying extents in the development of D-band antennas, particularly in antenna-in-package (AiP). CNC-machined (metallic) antennas yield high gain and low loss, but they are bulky, making integration with planar circuits challenging [3]. While 3D printing is suitable for planar designs, its high cost and relatively high surface roughness currently render it impractical for physically larger phased array or mass production [4]. LTCC technology has been validated for D-band applications [5], [6]. For example, a 4 × 4 antenna array that achieves a low profile and 12.5% bandwidth was designed [5]. However, LTCC technology is relatively costly and it can suffer from high feeding loss at the transition. Additionally, alternative materials such as bismaleimide-triazine (BT)-based organic substrates, glass, quartz, and benzocyclobutene (BCB) have been experimented for enhancing the radiation performance of wafer-layer packaging solutions [7]-[11]. Among these, BT-based organic substrates have gained favor for commercialization and mass production due to their affordable cost and mature processing techniques. In [7], a 4 × 2 antenna array design based on a four-layer BT organic substrate integrated waveguide (SIW) magneto-electric dipole antenna is proposed, delivering a peak gain of 14.1 dBi and stable broadside radiation performance. Moreover, a cavity-backed patch antenna etched on a silicon wafer and filled with BCB and Rogers 5880 can achieve a bandwidth of 32% [8]. However, the required back-cavity structure is relatively thick, with a thickness of 0.254 mm, which limits the potential for planar designs. Glass and quartz solutions can provide high efficiency and high-accuracy fabrication, but are not suitable for mass production [9], [10]. In [11], a single-layer microstrip-fed patch antenna utilizing BCB combined with four parasitic patch elements is presented. The antenna is attractive since it offers a bandwidth of 20% despite its simple single-layer design, but the design cannot be fabricated using current low-cost HDI PCB technology, which requires the trace and gap width to be above 50μm [12].

In this context, we propose a modified version of the D-band parasitic-loaded patch antenna [9], which also covers 20% bandwidth but can be manufactured using existing HDI PCB technology. While inspired by the previous design [9] and sharing some structural similarities (e.g., four grounded parasitic elements), the new antenna is designed from scratch using characteristic mode analysis (CMA) and has different operating principles [9]. The proposed antenna retains the simplicity of single-layer design, but superstrate loading is added to improve coupling to the parasitic elements, leading to the resonant modes and radiation characteristics being tuned for wideband operation.

II. Antenna Design and Analysis

Figure 1 shows the proposed superstrate-loaded parasitic patch antenna. The design utilizes Panasonic Megtron 8 PCB, consisting of one laminate R-5795 (ε_r = 3.19, tan δ = 0.0025) as the single-layer substrate and one prepreg R-5690 (ε_r = 3.23, tan δ = 0.0026) as the superstrate. The C-shaped patch and four parasitic elements are printed on the top of the substrate layer. The feedline is connected to the center of the inner side of the C-shaped patch, exciting the electrical field

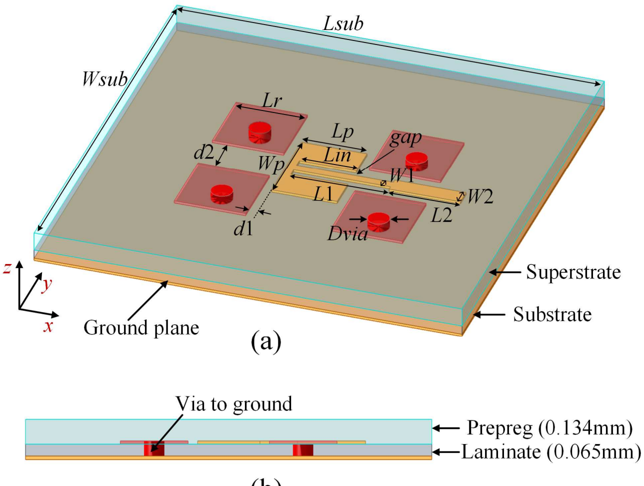

Fig. 1. Configuration of the proposed antenna. (a) Isometric view. (b) Side view.

TABLE I
OPTIMIZED PARAMETERS OF THE PROPOSED ANTENNA (Units: mm)

Parameters	*Wp*	*Lp*	*Lin*	*gap*	*W*1	*L*1
Value	0.63	0.46	0.4	0.06	0.06	0.68
Parameters	*W*2	*L*2	*Lr*	*d*1	*d*2	*Dvia*
Value	0.12	0.5	0.5	0.07	0.3	0.15

mode along the x-axis. The active C-shaped patch is also capacitively coupled to four surrounding square parasitic patches to enhance the bandwidth. The prepreg is laminated onto the patch as the superstrate to relax the fabrication requirement, improve the radiation efficiency, and further increase bandwidth. Table I provides the dimensions of the proposed antenna.

A. Design Principles and Procedure

Since the superstrate does not alter the fundamental operating principles of the antenna, this section will focus on the design of the antenna on the single-layer PCB substrate.

As shown in Fig. 2, Ant-1 is a conventional patch antenna, side-fed by a microstrip line. This basic design offers only one resonance, resulting in a narrow impedance bandwidth. Through characteristic mode analysis (CMA) using the integral solver of 2023 Altair FEKO, two resonant modes are identified for Ant-1, as depicted in Figs. 3 and 4(a). Mode 2 corresponds to the standard patch mode, whereas Mode 1 arises from the combined resonance of the patch and the feedline, producing a notch in the boresight radiation pattern. Mode 1 can be shifted out of the desired frequency band by extending the feedline line. In any case, the current feed point does not effectively excite the mode, with a large real part of input impedance. However, to minimize any negative influence of Mode 1 during the design process and to introduce a new resonance, Mode 1 is evolved into a new mode and utilized. To this end, adjustments are made to the insertion depth of the feedline, along with minor parameter modifications to the patch to retain the resonant frequencies

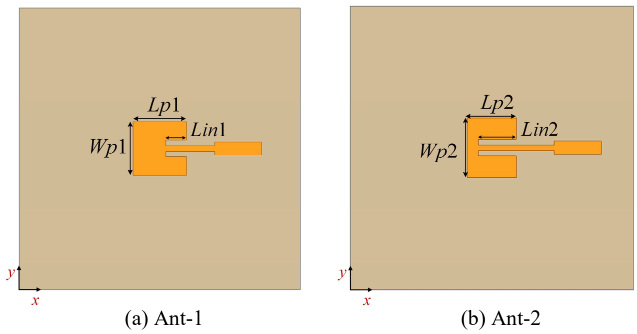

Fig. 2. Top view of the two antenna structures on a single board. ($Lp1$ = 0.57, $Wp1$ = 0.57, $Lin1$ = 0.22, $Lp2$ =0.51, $Wp2$ = 0.66, $Lin2$ = 0.4 . Unit: mm)

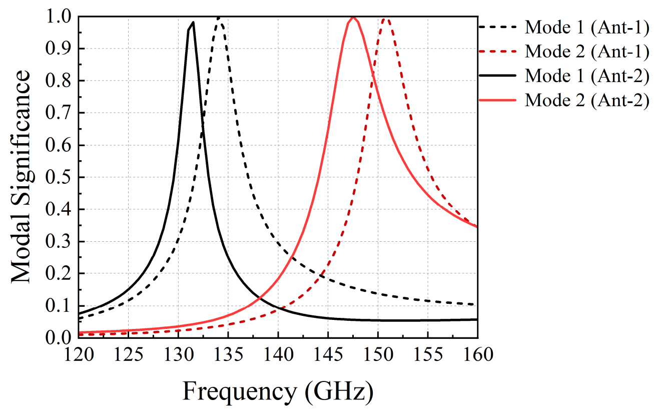

Fig. 3. Modal significance of excited modes for Ant-1 and Ant-2.

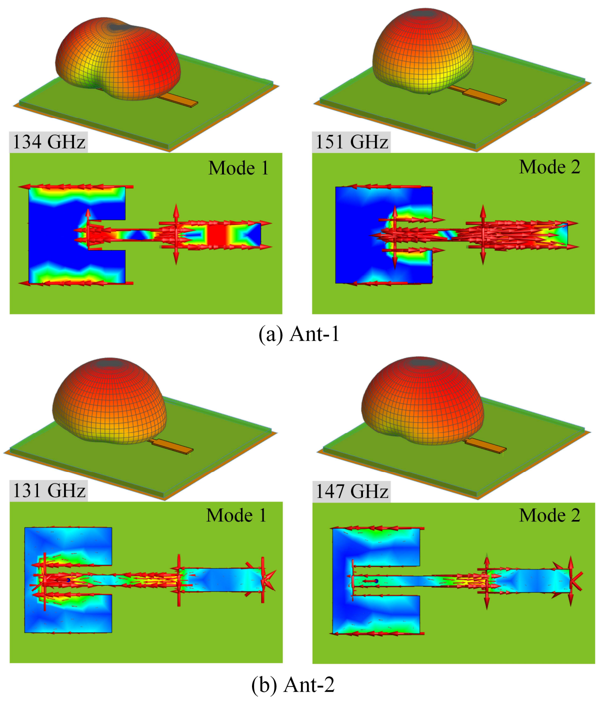

Fig. 4. Modal far-field radiation patterns and current distributions for (a) Ant-1 and (b) Ant-2.

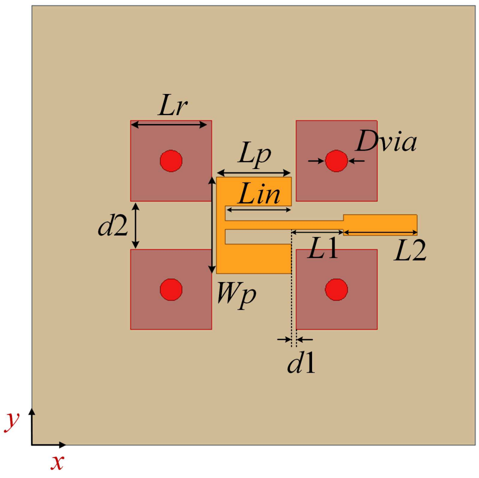

Fig. 5. Top view of the version of Ant-3. (Lp = 0.51, Wp = 0.66, Lr = 0.51, Lin = 0.45, $L1$ = 0.3, $L2$ = 0.5, $d1$ = 0.03, $d2$ = 0.33, $Dvia$ =0.15. Unit: mm)

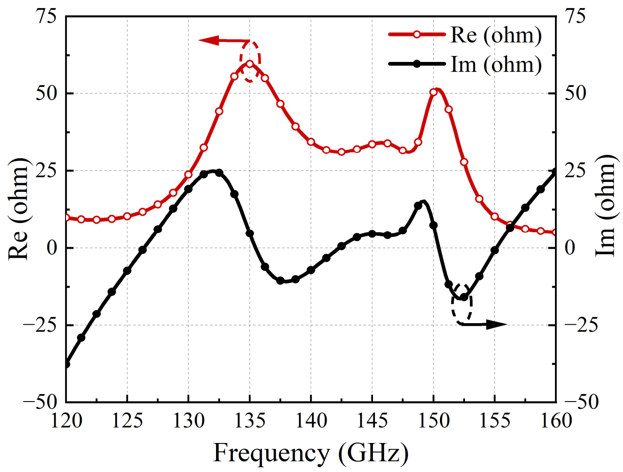

Fig. 6. Input impedance of Ant-3.

of the two modes. Ultimately, a C-shaped patch is formed, with both modes excited and matched to the feed (see Figs. 3 and 4(b)). In addition, the current distribution of the original Mode 1 has evolved such that the desired broadside pattern is obtained.

To further enhance the bandwidth, four parasitic patches are added around the C-shaped patch, which is utilized as the driven element (i.e., Ant-3, see Fig. 5). Each parasitic element is grounded at the center of the patch through a via with the diameter of 0.15 mm. Figure 6 provides the input impedance as obtained from the finite-element solver of 2023 Ansys HFSS, revealing three distinct resonances with real parts close to 50 Ω. The presence of these three resonances can be explained by the general equivalent circuits for Ant-1 to Ant-3 depicted in Fig. 7. A single patch (Ant-1) can be modeled as a parallel connection of resistance (R), capacitance (C), and inductance (L) [13]. In Ant-2, the longer feedline contributes to more inductance to the network, leading to the formation of an RLC resonance circuit. In Ant-3, the coupling capacitance between the edges of the central C-shaped patch

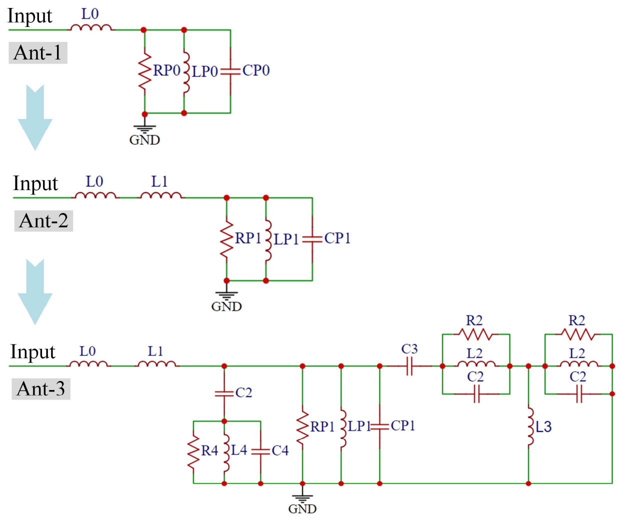

Fig. 7. The equivalent circuits of Ant-1, Ant-2 and Ant-3.

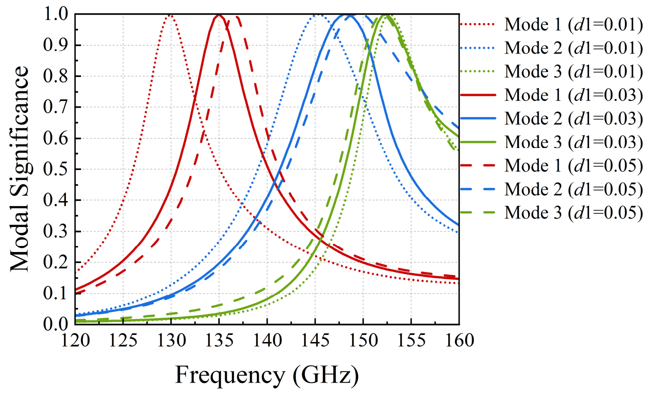

Fig. 8. Modal significance of three modes of Ant-3 as gap $d1$ varies.

and the parasitic patches, combined with the inductance introduced by the vias, creates another RLC resonant circuit, resulting in the emergence of a new resonance point. Furthermore, the parasitic elements interact with the feedline, giving rise to capacitive and inductive effects, which cause the left and right pairs of parasitic patches to show different operating behaviors.

If the same feeding method as Ant-1 is retained, only the modes with the electric field oriented along the x-axis can be excited. CMA reveals that Ant-3 can excite three distinct broadside modes, with the modal significance of these excited modes illustrated by the solid lines in Fig. 8 ($d1$ = 0.03 mm). The corresponding current distributions and far-field radiation patterns are presented in Fig. 9. The red solid line represents the mode identical to Mode 1 of Ant-2 (see Fig. 3), whose resonant frequency can be adjusted by modifying Lp and Lin. Mode 2 is mainly generated by the two parasitic patches on the left side, while Mode 3 is produced by the two parasitic patches on the right side. Notably, due to the coupling from the feedline on the two patches to the right, the current directions of Modes 2 and 3 are opposite. Hence, it is crucial to precisely control the frequencies of the two resonances to prevent mutual cancellation of the modes.

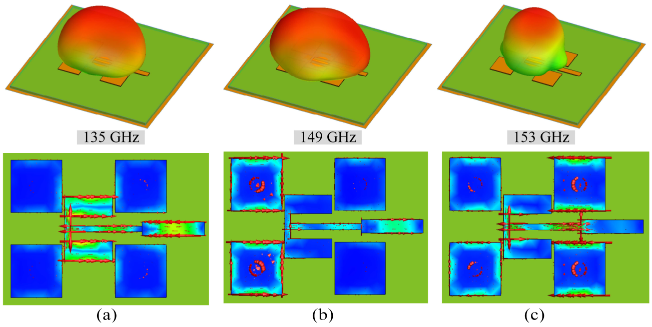

Fig. 9. Modal far-field radiation patterns and current distributions of Ant-3 for (a) Mode 1, (b) Mode 2, (c) Mode3.

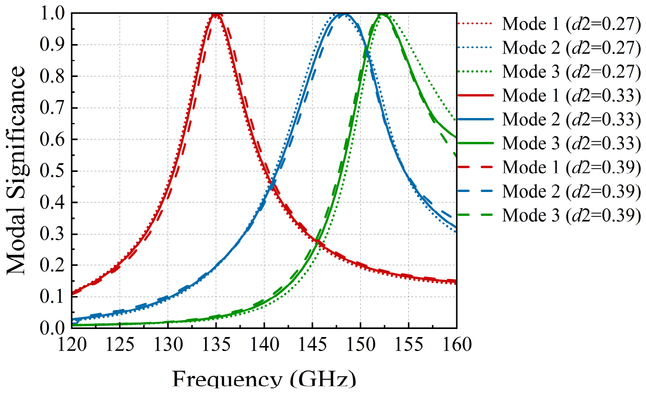

Fig. 10. Modal significance of three modes of Ant-3 as gap $d2$ varies.

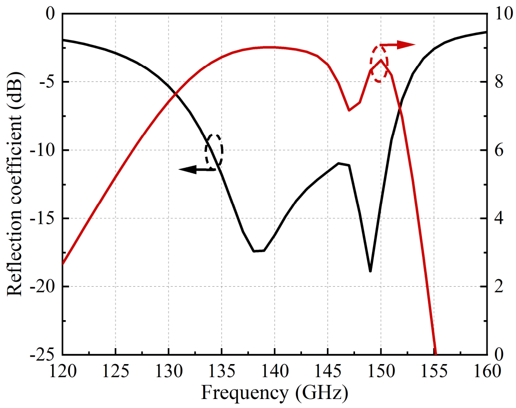

Fig. 11. Reflection coefficient and realized gain of Ant-3.

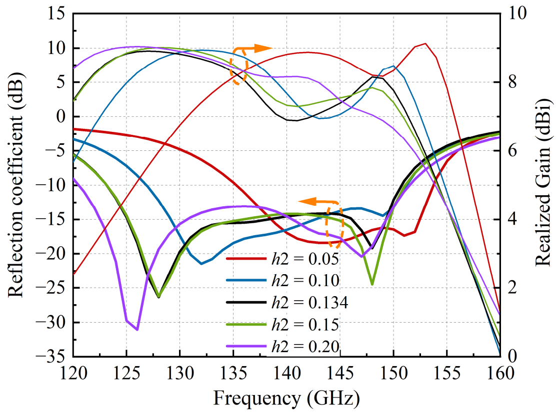

Fig. 12. Reflection coefficient and realized gain of superstrate-loaded antenna with varying superstrate thicknesses.

In addition, the gap between the parasitic patches and the C-shaped patch significantly impacts the wideband behavior, as it directly influences the resonant frequencies of Modes 1 and 2. As shown in Fig. 8, as the gap $d1$ increases from 0.01 mm (which reduces fabrication accuracy requirement), the coupling between the patches decreases, resulting in an effective shortening of the patches and increased resonant frequencies of Modes 1 and 2, while leaving the resonant frequency of Mode 3 relatively unchanged. This leads to a reduction in achievable bandwidth. At the same time, the resonant frequencies of Modes 2 and 3 gradually approach each other. Due to the opposite current directions of these two modes, destructive interference can occur between their far-field radiation fields. Therefore, determining the optimal gap size is essential.

On the other hand, the spatial separation between the left (or right) pair of parasitic patches along the y-axis ($d2$) has a much smaller influence on the modal resonances as compared to $d1$. In fact, the resonances are almost unchanged when $d2$ varies. However, as the parasitic patches move closer together, the coupling from the feedline to the left parasitic patch pair is enhanced. This is not beneficial since there is significant current in the feedline and it flows in the opposite direction to that of the currents on the parasitic patches, which negatively impacts the radiation performance. The optimized parameters of Ant-3 are provided in Fig. 5. Figure 11 shows that the structure of the optimized Ant-3 (evolved from Ant-1, a simple patch) features an enhanced 10 dB bandwidth of 11% (due to two additional modes) and 9 dBi peak gain. Moreover, only two resonances are seen, since the resonances of Modes 2 and 3 are in close proximity to each other (see Fig. 8). Nevertheless, this bandwidth is significantly lower than the previous design [9] and $d1$ = 0.03 mm is too small for fabrication with current HDI technology.

B. Practical Design Refinements

To enable fabrication with HDI technology, a gap size of $d1 \geq 0.05$ mm is required. To this end, a superstrate (prepreg R-5690, ε_r = 3.23, $\tan\delta$ = 0.0026) is added above the patches to more effectively confine the electric near-field within the dielectric, thereby enhancing the coupling between the active and parasitic patches (for a given gap size). This design allows for capacitive coupling to be retained at the same level even when the gap size is increased.

Figure 12 shows the impact of superstrate thickness $h2$ on the matching performance, for the chosen gap size of 0.07 mm. As the thickness increases, all three resonances of the antenna shift towards lower frequencies, while the bandwidth increases significantly. We selected the currently available maximum thickness of 0.134 mm for the prepreg R-5690 for the final design. The optimized antenna, with the parameters given in Table I, achieves a bandwidth of 20.2% and a maximum gain of 9 dBi. Figure 13 illustrates the radiation E-plane and H-plane patterns for the three resonant frequencies,

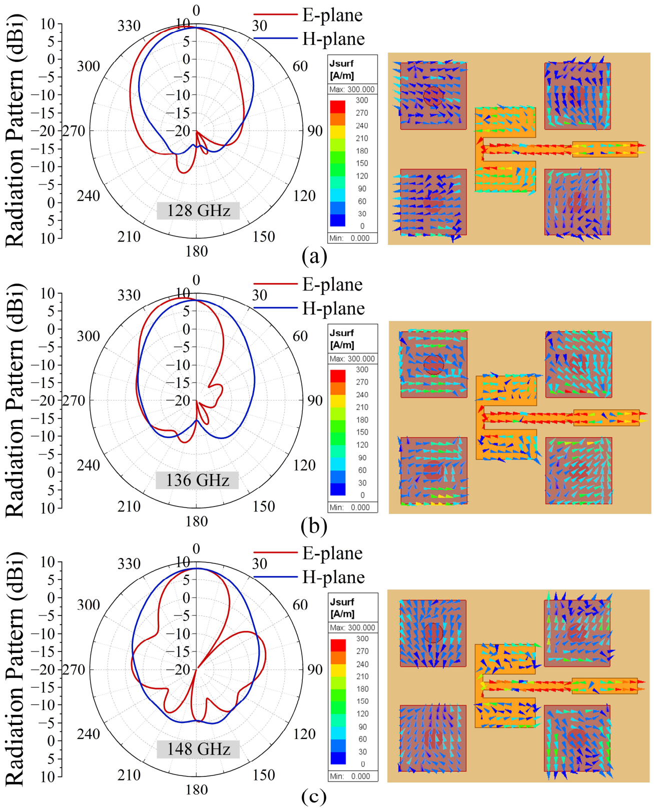

Fig. 13. E-plane and H-plane radiation patterns along with current distributions at (a) 128 GHz, (b) 136 GHz and (c) 148 GHz.

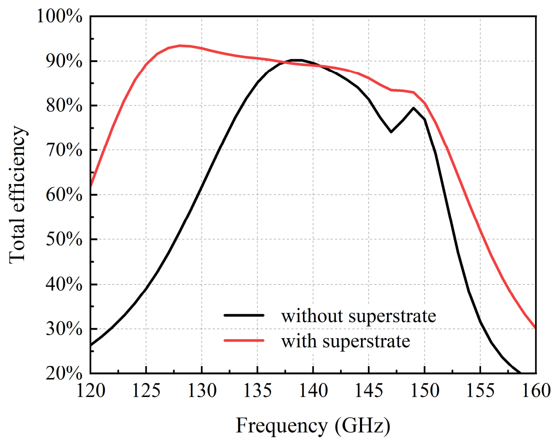

Fig. 14. Total efficiency of the proposed antenna with/without a superstrate.

along with the corresponding current distributions. Furthermore, the addition of the superstrate effectively yields high in-band total efficiency of ~80%-93%. To examine the effect of fabrication tolerance on $d1$, the performance impact was investigated for $d1 = 0.07 \pm 0.02$ mm. In the worst case of $d1 = 0.05$ mm, impedance matching degraded to 9 dB (with a 25% bandwidth) and the minimum realized gain decreased to 6 dBi.

III. Conclusions

This work presents a practical single-layer wideband D-band patch antenna loaded with four parasitic elements and a superstrate. It can achieve wideband performance and high gain using relatively low-cost fabrication with single-layer HDI PCB technology. Critical design parameters, particularly the gap between the parasitic patches and the C-shaped strip, were identified as essential for optimizing bandwidth and radiation characteristics. The integration of the superstrate significantly improved total efficiency, resulting in a bandwidth of 20.2% and a peak gain of 9 dBi, underscoring its potential for 6G wireless applications. Future work will include experimental validation of the proposed design.

Acknowledgment

This work is supported by the Horizon Europe (HEU) project 6GTandem.

References

[1] T. S. Rappaport, *et al.*, "Wireless communications and applications above 100 GHz: opportunities and challenges for 6G and beyond," *IEEE Access*, vol. 7, pp. 78729-78757, 2019.

[2] T. Dao, A. Kearns, D. Reyes Paredes, and G. Hueber, "Wideband high-gain stacked patch antenna array on standard PCB for D-Band 6G communications," *IEEE Antennas Wireless Propag. Lett.*, vol. 23, no. 2, pp. 478-482, Feb. 2024.

[3] D. Zarifi, A. Farahbakhsh, and A. U. Zaman, "A gap waveguide-based D-band slot array antenna with interdigital feed network," *IEEE Trans. Antennas Propag.*, vol. 71, no. 9, pp. 7124-7131, Sep. 2023.

[4] T. Merkle, R. Götzen, J. -Y. Choi, and S. Koch, "Polymer multichip module process using 3-D printing technologies for D-band applications," *IEEE Trans. Microw. Theory Tech.*, vol. 63, no. 2, pp. 481-493, Feb. 2015.

[5] S. Zhao, Y. Xu, and Y. Dong, "An LTCC-based antenna array for D-band terahertz communication," *IEEE Antennas Wireless Propag. Lett.*, vol. 22, no. 6, pp. 1491-1495, Jun. 2023.

[6] M. Ihle, S. Ziesche, C. Zech, and B. Baumann, "A broadband 140 GHz aperture-coupled SPA antenna in LTCC-technology," in *Proc. 53rd Europ. Microw. Conf. (EuMC)*, Berlin, Germany, 2023, pp. 327-330.

[7] H. C. Kuo, C. W. Kuo, C. C. Wang, and C-P. Hung, "A D-band magnetoelectric dipole antenna-in-package (AiP) implemented on BT-based organic substrate," *IEEE Trans. Comp. Package Manuf. Technol.*, vol. 12, no. 10, pp. 1673-1680, Oct. 2022.

[8] X. Wang, G. Xiao, B. Zhao, Y. Huang, and Q. Xu, "A broadband D-band cavity-backed coupled-feed patch antenna in wafer-level package based on heterogeneous integrations," *IEEE Trans. Antennas Propag.*, vol. 72, no. 8, pp. 6298-6308, Aug. 2024.

[9] H. Cheng, G. Xiao, and X. Wang, "A 123 GHz wideband patch antenna with parasitic modified mushroom structures," in *Proc. 10th IEEE Asia-Pacific Conf. Antennas Propag. (APCAP)*, Xiamen, China, 2022, pp. 1-2.

[10] S. Erdogan, K. -S. J. Moon, M. Kathaperumal, and M. Swaminathan, "D-band integrated and miniaturized quasi-Yagi antenna array in glass interposer," *IEEE Trans. Terahertz Sci. Technol.*, vol. 13, no. 3, pp. 270-279, May. 2023.

[11] L. Zhou, M. Tang, Z. Gao, J. Mao, H. Yue, and Y. Tang, "Design and fabrication of patch antenna array on quartz glass substrate at 146 GHz," in *Proc. 2020 Int. Conf. Microw. Mm Wave Technol.(ICMMT)*, Shanghai, China, 2020, pp. 1-3.

[12] A. Lamminen, J. Säily, J. Ala-Laurinaho, J. de Cos, and V. Ermolov, "Patch antenna and antenna array on multilayer high-frequency PCB for D-Band," *IEEE Open J. Antennas Propag.*, vol. 1, pp. 396-403, 2020.

[13] K. S. Kim, *et al.*, "A compact circular polarization antenna using folded ground elements," *IEEE Trans. Antennas Propag.*, vol. 67, no. 5, pp. 3472-3477, May. 2019.